Foveolar cone subtype patterning in human retinal organoids

Katarzyna A Hussey[1], Kiara Eldred[1,2], Thomas Reh[2], and Robert J. Johnston Jr[1]*

[1] Department of Biology, Johns Hopkins University, 3400 N. Charles Street, Baltimore, MD 21218, United States
[2] Department of Biological Structure, Institute for Stem Cells and Regenerative Medicine, University of Washington, Seattle, WA 98195, United States

* indicates corresponding author. Email: robertjohnston@jhu.edu

Key words: retina, foveola, cone, photoreceptor, organoid, retinoic acid, thyroid hormone, CYP26A1, DIO2, plasticity

Abstract

The mechanisms that generate patterns of cell types unique to humans are poorly understood. In the central region of the human retina, the high-acuity foveola is notable, in part, for its dense packing of green (M) and red (L) cones and absence of blue (S) cones. To identify mechanisms that promote M/L and suppress S cone patterning in the foveola, we examined human fetal retinas and differentiated human retinal organoids. During development, sparse S-opsin-expressing cones are observed in the foveola initially. Later, the foveola contains a mix of cones that either co-express S- and M/L-opsins or express M/L-opsin only. In adulthood, only M/L cones are present. Two signaling pathway regulators are highly and continuously expressed in the central retina: Cytochrome P450 26 subfamily A member 1 (CYP26A1) that degrades retinoic acid (RA) and Deiodinase 2 (DIO2) that promotes thyroid hormone (TH) signaling. C*YP26A1* null mutant organoids and high RA conditions increased S cones and limited M/L cones in human retinal organoids. Sustained TH signaling promoted the generation of M/L-opsin-expressing cones and induced M/L-opsin expression in S-opsin-expressing cones, showing that cone fate is plastic. Our data suggest that early CYP26A1 degrades RA to specify M/L cones and limit S cones and that continuous DIO2 expression sustains high levels of TH to convert S cones into M/L cones, yielding the M/L cone subtype patterning of the foveola. As the foveola is highly susceptible to impairment in diseases such as macular degeneration, a leading cause of vision loss, our findings inform organoid design for potential therapeutic applications.

Introduction

Visual acuity varies dramatically across the animal kingdom (Caves, Brandley, and Johnsen 2018). The high acuity of humans and primates is enabled by the foveola, a specialized region of the central macula (**Fig. 1A-C**). The human retina contains three subtypes of cones: S (short-wavelength, blue opsin), M (medium-wavelength, green opsin), and L (long-wavelength, red opsin) cones (Nathans, Thomas, and Hogness 1986). The foveola is characterized by a recessed pit containing a high density of M/L cones and the absence of S cones, rods, and vasculature (S. Polyak 1957; Willmer 1944; Willmer and Wright 1945; Wald 1967; Williams, MacLeod, and Hayhoe 1981). Whereas the macaque foveola contains a mix of M/L and S cone subtypes, the human foveola is uniquely comprised of exclusively M/L cones (**Fig. 1C**) (Keely Bumsted and Hendrickson

1999; K Bumsted et al. 1997). Here, we examined human fetal retinas and retinal organoids to determine mechanisms that generate the human-specific pattern of cone subtypes in the foveola.

Cone subtype specification occurs in a two-step process. First, a decision occurs between S and M/L cone fates. If the M/L fate is chosen, a decision is made between M and L fates (Vollrath, Nathans, and Davis 1988; Wang et al. 1992; Smallwood, Wang, and Nathans 2002; Wang et al. 1999). As the adult human foveola is composed of M and L cones and lacks S cones, we focused on the decision between S and M/L fates.

In the developing human retina, cone subtype specification initiates in the center and expands to the periphery. S-opsin-expressing cones are first observed in the central retina at fetal week 10. The region containing S-opsin-expressing cones spreads in a wave of differentiation until the entire retina contains S-opsin-expressing cones by fetal week 22 (Xiao and Hendrickson 2000; Cornish, Hendrickson, and Provis 2004). M/L-opsin-expressing cones are first observed in the central retina at fetal week 14. M/L cone subtype specification expands to the periphery until the entire retina contains M/L-opsin expressing cones postnatally (Cornish, Hendrickson, et al., 2004). Though the presumptive foveola contains S-opsin-expressing cones during fetal development (Xiao and Hendrickson 2000), the adult foveola contains M/L cones exclusively (Willmer 1944; Willmer and Wright 1945; Wald 1967; Williams, MacLeod, and Hayhoe 1981). Based on the observation that the foveola undergoes an increase in cone density in the absence of local cell division, Diaz-Araya and Provis proposed that M/L cones migrate into the foveola, pushing S cones out (Diaz Araya and Provis 1992). The absence of an experimentally amenable human model system has limited interrogation of this hypothesis and the mechanisms controlling foveolar cone subtype patterning.

Co-expression of S- and M/L-opsins was observed in the fovea and at the edge of the wave of M/L-opsin expression during fetal eye development (Xiao and Hendrickson 2000; Cornish et al. 2004), suggesting potential plasticity in cone subtype fate. Here we test an alternative hypothesis that patterning of the M/L cone-rich foveola is generated by limited S cone specification and conversion of sparse S cones into M/L cones.

While the foveola is unique to primates among mammals, some bird species have analogous high-acuity areas (HAA). Foundational studies in chicken found that CYP26A1, an RA-degrading enzyme, is expressed in the developing HAA. Aberrant RA disrupts HAA development (da Silva and Cepko 2017), showing that low levels of RA signaling are critical for the patterning of HAAs. Expression of CYP26A1 in the central retina is conserved in the developing and adult human retina (da Silva and Cepko 2017; Peng et al. 2019; Lu et al. 2020; Yi et al. 2020; Cowan et al. 2020), suggesting a role for RA degradation in cone subtype patterning in the human foveola.

We previously found that TH signaling controls the S vs. M/L cone fate choice using human retinal organoids (Eldred et al. 2018). Retinal organoids recapitulate what is known about the temporal specification of cone subtypes and morphologies (Eldred et al. 2018; Nakano et al. 2012; Wahlin et al. 2017; Kaewkhaw et al. 2015). Our study suggested that dynamic expression of TH-degrading and -activating proteins ensures low signaling early to specify S cones and high signaling late to produce M/L cones. Notably, expression of DIO2, an enzyme that converts circulating T4 thyroid hormone to active T3, increases during human fetal retinal and organoid development, consistent with high TH signaling and specification of M/L cones later in development (Eldred et al. 2018; Hoshino

et al. 2017). Whereas *DIO2* expression decreases in the peripheral retina by adulthood, expression of *DIO2* is maintained at high levels in the central retina (Lu et al. 2020; Yi et al. 2020), suggesting that continuous *DIO2* expression and sustained TH signaling play a role in M/L-only cone patterning in the foveola.

In this study, we examined cone opsin expression in fetal retinas and found that S-opsin-expressing cones are observed sparsely in the central retina early in development, suggesting mechanisms to limit their local specification. Later in fetal development, cones in the central retina either express M/L-opsin exclusively or co-express S-opsin and M/L-opsin. By adulthood, this region contains only M/L cones, suggesting that the initial sparse S-opsin-expressing cones convert into M/L cones. Based on the expression of CYP26A1 and DIO2 in the foveola, we tested the roles of RA and TH signaling on cone subtype specification in retinal organoids. Our experiments suggest that RA is degraded to promote the specification of M/L cones and limit the generation of S cones in the foveola, and that sustained TH signaling is sufficient to convert S cones to the M/L cone fate, indicating plasticity of cone subtypes. Our data suggest that cell fate specification and conversion mechanisms pattern cone subtypes in the human foveola.

Results

Cone subtype patterning in the developing foveola

We examined opsin expression in human fetal retinas to describe the developmental dynamics of foveolar cone subtype pattering. Previous studies characterized S-opsin and M/L-opsin expression during development and identified a population of co-expressing cells through double-exposure imaging (Cornish et al. 2004; Xiao and Hendrickson 2000; Keely Bumsted and Hendrickson 1999). To understand the patterning of cone subtypes, we utilized immunohistochemistry and confocal microscopy to image opsin expression in wholemount fetal retinas. We examined M/L-opsin with an antibody that detects both M- and L-opsin due to their extremely high protein sequence identity (Nathans, Thomas, and Hogness 1986). At 8 weeks of gestation, we did not observe expression of cone opsins (data not shown), consistent with previous observations (Xiao & Hendrickson, 2000). At all later timepoints, we observed cells that expressed S-opsin exclusively, M/L-opsin exclusively, or both S-opsin and M/L-opsin (**Fig. 1D-R**). For each timepoint, we quantified the number of opsin-expressing cells in 300 µm by 300 µm regions, which is approximately the size of the adult S cone-free foveola (Curcio et al. 1991; 1990; Hendrickson 1992; S. L. Polyak 1941).

We next examined retinas at 10, 12, 14, and 16 weeks of gestation (**Fig. 1E-R)**. At gestational week 10, S-opsin-expressing cones were observed in a 990 µm by 450 µm ellipsoid area encompassing the presumptive foveola. To define the range of S-opsin-expressing cone densities, we quantified the regions within this area that contained the greatest and least cones/mm^2. The lowest density region contained 0 cones/mm^2 and the highest density region contained 100 cones/mm^2 (**Fig. 1E-H; Fig. S1A**). The average cone density of the entire region of S-opsin-expressing cones was 38 cones/mm^2 (**Fig. 1G**). As the overall density of S-opsin-expressing cones was low at this timepoint, we could not determine if the region lacking S-opsin-expressing cones was the presumptive foveola or a result of random variation in the low-density cell pattern.

At gestational week 12, S-opsin-expressing cones covered a region of 1940 µm

by 1530 µm, encompassing the presumptive foveola. The lowest density region contained 100 cones/mm^2 and the highest density region contained 389 cones/mm^2 (**Fig. 1I-L; Fig. S1B**). The average cone density of the entire region of S-opsin-expressing cones was 218 cones/mm^2 (**Fig. 1K**). The observation of S-opsin-expressing cones throughout all regions suggested that sparse S-opsin-expressing cones are present in the presumptive foveola at this developmental timepoint.

At gestational week 14, we observed cells that expressed S-opsin exclusively, M/L-opsin exclusively, or co-expressed S-opsin and M/L-opsin. A central region encompassing the presumptive foveola contained cones that expressed M/L-opsin exclusively (**Fig. 1M-O, "Z1"; Fig. S1C**). The neighboring region contained a mix of cones that expressed M/L-opsin exclusively, expressed S-opsin exclusively, or co-expressed S-opsin and M/L-opsin (**Fig. 1M-O, "Z2"; Fig. S1C**). In the most peripheral area, a region contained cones that expressed S opsin exclusively (**Fig. 1M-O, "Z3"; Fig. S1C**).

At gestational week 16, we similarly observed cells that expressed S-opsin exclusively, M/L-opsin exclusively, or co-expressed S-opsin and M/L-opsin. The central region encompassing the presumptive foveola mostly contained cones that expressed M/L-opsin with some cones that co-expressed S-opsin and M/L-opsin and very rare cones that expressed S-opsin exclusively (**Fig. 1P-R, "Z1"; Fig. S1D**). In the four neighboring regions, most cones expressed M/L-opsin exclusively. A proportion of cones expressed S-opsin exclusively or co-expressed S- and M/L-opsin. The proportion of S-opsin-expressing cones increased with the distance from the center (**Fig. 1P-R, "Z2"-"Z5"; Fig. S1D**). A distal region starting at 2.3 mm from the presumptive foveola contained only S-opsin-expressing cones (**Fig. 1P-R, "Z6"; Fig. S1D**). The presence of S-opsin-expressing cones in the central region suggested that sparse S-opsin-expressing cones are present in the presumptive foveola and most, if not all, S-opsin-expressing cones undergo a period of co-expression with M/L-opsin.

We compared our findings in fetal human retinas to the distribution of cone subtypes in an adult human retina. We quantified cone subtype ratios at various regions beginning near the foveola and moving toward the peripheral retina (**Fig. S1E-H**). Due to the whole mount imaging approach, cone patterning in the foveola was not detectable. At central regions, the retina contained mostly M/L cones (**Fig. S1E, F, I, J**). Towards the periphery, S cones increased in proportion and density (**Fig. S1E, G-J**). Cones that co-expressed S-opsin and M/L-opsin were not observed in the adult retina (**Fig. S1E-J**), suggesting that the co-expression of opsins observed in fetal retinal development is transient.

Our observations suggest that sparse S cones specified in the foveola initially express S-opsin exclusively, then co-express M/L-opsin, and finally express M/L-opsin and adopt the M/L cone fate (**Fig. 1S**). Outside of the foveola, it appears that S cones initially express S-opsin exclusively, then co-express S-opsin and M/L-opsin, and ultimately revert to expressing S-opsin only (**Fig. 1S**).

Our results are consistent with previous observations of cone subtypes in the central retina during fetal development (Xiao and Hendrickson 2000; Cornish, Hendrickson, and Provis 2004). Our experiments validated the presence of S-opsin-expressing cells in the presumptive foveola and assessed the spatial distribution of cones that co-express S-opsin and M/L-opsin. Apoptosis is not readily observed in photoreceptors in the fetal retina, suggesting that the decrease in co-expressing cones is

not due to cell death (Cornish et al. 2004). Based on these observations, we hypothesized that S cone specification is limited in the foveola and that the sparse, remaining S cones are converted into M/L cones.

Organoids contain cones that co-express S-opsin and M/L-opsin

We next examined opsin expression in human retinal organoids. To internally control for batch effects and limit variability, organoids were differentiated at the same time for each experiment. Organoids at day 80 contained cones that expressed S-opsin exclusively (**Fig. S2A, S2D-E**). Organoids at day 100 contained cones that expressed S-opsin exclusively or co-expressed S-opsin and M/L-opsin (**Fig. S2D-E**). Organoids at day 110 and day 130 contained cones that expressed S-opsin exclusively, expressed M/L-opsin exclusively, or co-expressed S-opsin and M/L-opsin (**Fig. S2B, S2D-E**). Organoids on days 152, 170, and 190 contained cones that expressed S-opsin exclusively or M/L-opsin exclusively (**Fig. S2C-E**). These data suggested two nonexclusive mechanisms of cone subtype development in organoids: (1) S cones express S-opsin exclusively, then co-express S-opsin and M/L-opsin, and finally, revert to expressing S-opsin exclusively, or (2) S cones express S-opsin exclusively, then co-express S-opsin and M/L-opsin, and convert to M/L cones. Both possibilities are consistent with our observations of cone development in human fetal retinas.

CYP26A1 and low RA promote M/L cone fate and suppress S cone fate

We next sought to identify a mechanism that limits the generation of S-opsin-expressing cones in the foveola. The RA-degrading enzyme CYP26A1 is expressed in the central retina (Cowan et al. 2020; Yi et al. 2020; Lu et al. 2020; da Silva and Cepko 2017; Peng et al. 2019). Low RA signaling is required to pattern the HAA in chicken (da Silva and Cepko 2017). Based on these observations, we hypothesized that CYP26A1 and low RA promote M/L cone fate and suppress S cone fate.

To investigate the role of CYP26A1 in cone subtype specification, we generated a *CYP26A1* null mutation in human embryonic stem cells (**Fig. S2F-G**). We grew wildtype and *CYP26A1* null mutant retinal organoids and examined cone subtypes at day 204. Whereas wildtype organoids displayed 98% M/L cones and 2% S cones, *CYP26A1* null mutant organoids displayed 77% M/L cones and 23% S cones (**Fig. 2A-C**), suggesting that CYP26A1 promotes M/L cone fate and suppresses S cone fate. Wildtype organoids had a higher density of total cones compared to *CYP26A1* null mutants (**Fig. 2D**), suggesting that CYP26A1 likely also promotes cone generation, consistent with the high cone density in the foveola.

As CYP26A1 degrades RA, we directly tested how levels of RA signaling affect cone subtype specification by growing organoids in different RA concentrations. We found that as RA concentration increased, the proportion of S cones increased and the proportion of M/L cones decreased at day 213 (**Fig. 2F-I**). The density of cones was not significantly different across the range of RA concentrations (**Fig. S2H**), suggesting that constant exogenous RA may affect cone development differently than endogenous CYP26A1-mediated regulation. These observations suggest that low RA promotes M/L cone specification and suppresses S cone specification.

Together, these data suggest that CYP26A1 and low RA suppress S cones and promote M/L cones, consistent with CYP26A1 expression in the central retina and the

limited specification of S cones in the foveola (**Fig. 2E**).

Sustained TH signaling converts S cones into M/L cones

Analyses of fetal retinas suggested that S-opsin-expressing cones in the foveola convert to M/L cone fate (**Fig. 1E-R**) (Cornish et al. 2004; Xiao and Hendrickson 2000). We previously showed that TH signaling is necessary and sufficient to promote M/L cone fate and suppress S cones (Eldred et al. 2018). DIO2, which promotes TH signaling, is expressed at high levels in the central retina through adulthood (Lu et al. 2020). Based on this continuous expression of DIO2, we hypothesized that sustained TH signaling converts S cones into M/L cones.

We previously grew human retinal organoids in high active T3 media conditions throughout their development from day 22 to day 200 and observed a high proportion of M/L cones and a low proportion of S cones (Eldred et al., 2018). These experiments were conducted in 1 μM RA through day 130, resulting in a delay in cone specification, an increase in the proportion of S cones, and a decrease in the proportion of M/L cones (Eldred et al., 2018). For comparison to these observations, we similarly grew organoids in 1 μM RA through day 130 for the next experiments.

To assess how timing and duration of TH signaling influences cone subtype specification, we grew human retinal organoids and varied when we started or ended a pulse of high T3. We defined five key developmental timepoints: before cone generation (day 22), when S-opsin is first detected (day 152), when M/L-opsin is first detected (day 171), after both S and M/L cones are generated (day 190), and when opsin expression and cone subtype fates are assessed (day 200) (Eldred et al., 2018). As the time-off and time-on experiments were conducted simultaneously, the control organoids grown in the absence of supplemental T3 and the organoids grown in continuous T3 on days 22-200 were the same for both experiments (**Fig. 3A-F**).

We first varied when the high T3 pulse was ended. Control organoids grown in the absence of supplemental T3 contained a mix of S and M/L with very sparse co-expressing cones (**Fig. 3A, 3E-F**). Organoids grown in high T3 conditions throughout development from days 22-200 were M/L cone-rich (**Fig. 3B, E-F**) consistent with our previous observations (Eldred et al. 2018). Organoids grown in high T3 conditions beyond S and M/L cone generation from days 22-190 similarly were M/L cone-rich (**Fig. 3E**). Organoids grown in high T3 beyond S cone generation but before M/L cone generation (days 22-171) contained a mix of cones that expressed M/L-opsin exclusively, co-expressed S-opsin and M/L-opsin, or expressed S-opsin exclusively (**Fig. 3E**). Similarly, organoids grown in high T3 until the initiation of S cone generation (days 22-152) contained a mix of cones that expressed M/L-opsin exclusively, co-expressed S-opsin and M/L-opsin, or expressed S-opsin exclusively (**Fig. 3C, E**). Adding T3 for extended time windows (day 22-200, 22-190) yielded M/L cone-rich organoids, suggesting that sustained T3 promotes the generation of M/L cones and suppression of S cones. Adding T3 for shorter periods (day 22-171, day 22-152) generated organoids with cones that co-expressed S-opsin and M/L-opsin, suggesting that a shorter pulse of T3 promotes S cones to take on M/L cone features.

We next varied when the high T3 conditions were started. Organoids grown in high T3 starting at the initiation of S cone generation (days 152-200) were M/L cone-rich (**Fig. 3F**), suggesting that initiating and sustaining high T3 before S cone generation promotes

the specification of M/L cones and suppression of S cones. Organoids grown in high T3 starting after the initiation of S cone generation but before the generation of M/L cones (days 171-200) were M/L cone-rich (**Fig. 3F**), suggesting that T3 is sufficient to promote M/L cones and convert S cones into M/L cones after S cone generation. Organoids grown in high T3 conditions after the generation of S and M/L cones from days 190-200 contained a mix of cones that expressed M/L opsin exclusively, co-expressed S-opsin and M/L-opsin, or expressed S-opsin exclusively (**Fig. 3D, 3F**), suggesting that T3 induces M/L-opsin expression in S cones during this short pulse of T3 and is not sustained long enough to convert all S cones fully to the M/L cone fate. Together, these data suggest that sustained T3 promotes the generation of M/L cones and the conversion of S cones into M/L cones.

Discussion

We investigated the patterning of cone subtypes in the human foveola. The foveola initially contains sparse S-opsin-expressing cones. During fetal development, the foveola contains cones that express M/L-opsin only or co-express S-opsin and M/L-opsin. By adulthood, all cones in the foveola express M/L-opsin exclusively (Willmer 1944; Willmer and Wright 1945; Wald 1967; Williams, MacLeod, and Hayhoe 1981). *CYP26A1* mutants and high RA conditions yielded organoids with increased S cones, whereas wild type and low RA conditions resulted in organoids with increased M/L cones. While sustained high levels of T3 generated M/L cone-rich organoids, pulses of T3 yielded organoids with cones that co-expressed S- and M/L-opsin. Together, these data suggest that CYP26A1 degrades RA to limit S cone generation (**Fig. 4A**) and sustained DIO2 and T3 signaling convert sparse S cones into M/L cones (**Fig. 4B**), to generate the M/L cone-rich pattern in the foveola (**Fig. 4C**).

Our findings for the roles of RA and TH in human cone subtype specification and conversion are consistent with observations from other species. In mice, expression of CYP26A1 is restricted to a stripe in the central retina by the VAX2 transcription factor. In VAX2 knockouts, the expression domain of CYP26A1 is expanded, as is the region containing M cones into the predominantly S cone rich ventral dorsal retina (Alfano et al. 2011), consistent with the role of CYP26A1 in promoting M/L and limiting S cone fate in human retinal organoids.

Opsin expression switching has been observed in several species. In salmonids, TH controls switching of opsin expression from UV opsin to blue opsin during smoltification (Gan and Novales Flamarique 2010; Cheng, Gan, and Flamarique 2009; McNerney and Johnston 2021). In flies, ecdysone hormone mediates a blue to green switch in opsin expression in photoreceptors of the Bolwig organ during the transition from larval to adult development (Sprecher and Desplan 2008). The rat and gerbil retinas also undergo periods of opsin co-expression at the onset of M cone specification, which resolves as the animals mature, though the mechanisms are not understood (Szél, van Veen, and Röhlich 1994). These observations are consistent with our finding that sustained TH signaling switches S cones to M/L cone fate in humans.

Our studies show that organoids can be used to model and study human-specific regional patterning of the retina. Our findings have important implications for developing therapies for retinal degenerative diseases, including macular degeneration. While current therapies slow disease progression (Guymer et al. 2019; Chandra et al. 2020;

CATT Research Group et al. 2011; Wecker et al. 2019; Age-Related Eye Disease Study 2 Research Group 2013; Age-Related Eye Disease Study Research Group 2001), there is no cure. Transplantation approaches could be improved using retinal organoids with specific ratios of photoreceptors that match the transplanted region. Our work identified genetic and pharmacological manipulations that pattern cone subtypes in organoids similar to the high-acuity foveola. As the foveola is highly susceptible to impairment in diseases including macular degeneration, our findings inform organoid design for potential therapeutic applications.

Acknowledgements:

Human tissue was obtained from the University of Maryland Brain and Tissue Bank, which is a Brain and Tissue Repository of the NIH Neurobiobank, and the National Disease Research Interchange (NDRI). Lukas Voortman generated 10 and 12 week fetal S cone heatmaps.

References

Age-Related Eye Disease Study 2 Research Group. 2013. “Lutein + Zeaxanthin and Omega-3 Fatty Acids for Age-Related Macular Degeneration: The Age-Related Eye Disease Study 2 (AREDS2) Randomized Clinical Trial.” *JAMA* 309 (19): 2005–15. https://doi.org/10.1001/jama.2013.4997.

Age-Related Eye Disease Study Research Group. 2001. “A Randomized, Placebo-Controlled, Clinical Trial of High-Dose Supplementation with Vitamins C and E, Beta Carotene, and Zinc for Age-Related Macular Degeneration and Vision Loss: AREDS Report No. 8.” *Archives of Ophthalmology (Chicago, Ill. : 1960)* 119 (10): 1417–36. https://doi.org/10.1001/archopht.119.10.1417.

Alfano, Giovanna, Ivan Conte, Tiziana Caramico, Raffaella Avellino, Benedetta Arnò, Maria Teresa Pizzo, Naoyuki Tanimoto, et al. 2011. “*Vax2* Regulates Retinoic Acid Distribution and Cone Opsin Expression in the Vertebrate Eye.” *Development* 138 (2): 261–71. https://doi.org/10.1242/dev.051037.

Bumsted, K, C Jasoni, A Szél, and A Hendrickson. 1997. “Spatial and Temporal Expression of Cone Opsins during Monkey Retinal Development.” *The Journal of Comparative Neurology* 378 (1): 117–34.

Bumsted, Keely, and Anita Hendrickson. 1999. “Distribution and Development of Short-Wavelength Cones Differ Between Macaca Monkey and Human Fovea.” *J. Comp. Neurol*. Vol. 403.

CATT Research Group, Daniel F Martin, Maureen G Maguire, Gui-shuang Ying, Juan E Grunwald, Stuart L Fine, and Glenn J Jaffe. 2011. “Ranibizumab and Bevacizumab for Neovascular Age-Related Macular Degeneration.” *The New England Journal of Medicine* 364 (20): 1897–1908. https://doi.org/10.1056/NEJMoa1102673.

Caves, Eleanor M., Nicholas C. Brandley, and Sönke Johnsen. 2018. “Visual Acuity and the Evolution of Signals.” *Trends in Ecology & Evolution* 33 (5): 358–72. https://doi.org/10.1016/j.tree.2018.03.001.

Chandra, Shruti, Cristina Arpa, Deepthy Menon, Hagar Khalid, Robin Hamilton, Luke Nicholson, Bishwanath Pal, et al. 2020. “Ten-Year Outcomes of Antivascular Endothelial Growth Factor Therapy in Neovascular Age-Related Macular Degeneration.” *Eye* 34 (10): 1888–96. https://doi.org/10.1038/s41433-020-0764-9.

Cheng, Christiana L., Kathlyn J. Gan, and In~igo Novales Flamarique. 2009. “Thyroid Hormone Induces a Time-Dependent Opsin Switch in the Retina of Salmonid Fishes.” *Investigative Opthalmology & Visual Science* 50 (6): 3024. https://doi.org/10.1167/iovs.08-2713.

Cornish, Elisa E., Anita E. Hendrickson, and Jan M. Provis. 2004. “Distribution of Short-Wavelength-Sensitive Cones in Human Fetal and Postnatal Retina: Early Development of Spatial Order and Density Profiles.” *Vision Research* 44 (17): 2019–26. https://doi.org/10.1016/j.visres.2004.03.030.

Cornish, Elisa E., Ming Xiao, Zhantao Yang, Jan M. Provis, and Anita E. Hendrickson. 2004. “The Role of Opsin Expression and Apoptosis in Determination of Cone Types in Human Retina.” *Experimental Eye Research* 78 (6): 1143–54. https://doi.org/10.1016/j.exer.2004.01.004.

Cowan, Cameron S., Magdalena Renner, Martina de Gennaro, Brigitte Gross-Scherf, David Goldblum, Yanyan Hou, Martin Munz, et al. 2020. “Cell Types of the Human

Retina and Its Organoids at Single-Cell Resolution." *Cell* 182 (6): 1623-1640.e34. https://doi.org/10.1016/j.cell.2020.08.013.
Curcio, Christine A., Kimberly A. Allen, Kenneth R. Sloan, Connie L. Lerea, James B. Hurley, Ingrid B. Klock, and Ann H. Milam. 1991. "Distribution and Morphology of Human Cone Photoreceptors Stained with Anti-Blue Opsin." *The Journal of Comparative Neurology* 312 (4): 610–24. https://doi.org/10.1002/cne.903120411.
Curcio, Christine A., Kenneth R. Sloan, Robert E. Kalina, and Anita E. Hendrickson. 1990. "Human Photoreceptor Topography." *The Journal of Comparative Neurology* 292 (4): 497–523. https://doi.org/10.1002/cne.902920402.
Diaz Araya, Claudia, and Jan M. Provis. 1992. "Evidence of Photoreceptor Migration during Early Foveal Development: A Quantitative Analysis of Human Fetal Retinae." *Visual Neuroscience* 8 (6): 505–14. https://doi.org/10.1017/S0952523800005605.
Eldred, Kiara C., Sarah E. Hadyniak, Katarzyna A. Hussey, Boris Brenerman, Ping-Wu Zhang, Xitiz Chamling, Valentin M. Sluch, et al. 2018. "Thyroid Hormone Signaling Specifies Cone Subtypes in Human Retinal Organoids." *Science* 362 (6411). https://doi.org/10.1126/science.aau6348.
Gan, Kathlyn J., and Iñigo Novales Flamarique. 2010. "Thyroid Hormone Accelerates Opsin Expression during Early Photoreceptor Differentiation and Induces Opsin Switching in Differentiated TRα-Expressing Cones of the Salmonid Retina." *Developmental Dynamics* 239 (10): 2700–2713. https://doi.org/10.1002/dvdy.22392.
Guymer, Robyn H., Zhichao Wu, Lauren A.B. Hodgson, Emily Caruso, Kate H. Brassington, Nicole Tindill, Khin Zaw Aung, et al. 2019. "Subthreshold Nanosecond Laser Intervention in Age-Related Macular Degeneration." *Ophthalmology* 126 (6): 829–38. https://doi.org/10.1016/j.ophtha.2018.09.015.
Hendrickson, Anita. 1992. "A Morphological Comparison of Foveal Development in Man and Monkey." *Eye* 6 (2): 136–44. https://doi.org/10.1038/eye.1992.29.
Hoshino, Akina, Rinki Ratnapriya, Matthew J. Brooks, Vijender Chaitankar, Matthew S. Wilken, Chi Zhang, Margaret R. Starostik, et al. 2017. "Molecular Anatomy of the Developing Human Retina." *Developmental Cell* 43 (6): 763-779.e4. https://doi.org/10.1016/j.devcel.2017.10.029.
Kaewkhaw, Rossukon, Koray Dogan Kaya, Matthew Brooks, Kohei Homma, Jizhong Zou, Vijender Chaitankar, Mahendra Rao, and Anand Swaroop. 2015. "Transcriptome Dynamics of Developing Photoreceptors in Three-Dimensional Retina Cultures Recapitulates Temporal Sequence of Human Cone and Rod Differentiation Revealing Cell Surface Markers and Gene Networks." *Stem Cells* 33 (12): 3504–18. https://doi.org/10.1002/stem.2122.
Lu, Yufeng, Fion Shiau, Wenyang Yi, Suying Lu, Qian Wu, Joel D. Pearson, Alyssa Kallman, et al. 2020. "Single-Cell Analysis of Human Retina Identifies Evolutionarily Conserved and Species-Specific Mechanisms Controlling Development." *Developmental Cell* 53 (4): 473-491.e9. https://doi.org/10.1016/j.devcel.2020.04.009.
McNerney, Christina, and Robert J. Johnston. 2021. "Thyroid Hormone Signaling Specifies Cone Photoreceptor Subtypes during Eye Development: Insights from

Model Organisms and Human Stem Cell-Derived Retinal Organoids." In , 51–90. https://doi.org/10.1016/bs.vh.2021.03.001.
Nakano, Tokushige, Satoshi Ando, Nozomu Takata, Masako Kawada, Keiko Muguruma, Kiyotoshi Sekiguchi, Koichi Saito, Shigenobu Yonemura, Mototsugu Eiraku, and Yoshiki Sasai. 2012. "Self-Formation of Optic Cups and Storable Stratified Neural Retina from Human ESCs." *Cell Stem Cell* 10 (6): 771–85. https://doi.org/10.1016/j.stem.2012.05.009.
Nathans, Jeremy, Darcy Thomas, and David S. Hogness. 1986. "Molecular Genetics of Human Color Vision: The Genes Encoding Blue, Green, and Red Pigments." *Science* 232 (4747): 193–202. https://doi.org/10.1126/science.2937147.
Peng, Yi-Rong, Karthik Shekhar, Wenjun Yan, Dustin Herrmann, Anna Sappington, Gregory S. Bryman, Tavé van Zyl, Michael Tri. H. Do, Aviv Regev, and Joshua R. Sanes. 2019. "Molecular Classification and Comparative Taxonomics of Foveal and Peripheral Cells in Primate Retina." *Cell* 176 (5): 1222-1237.e22. https://doi.org/10.1016/j.cell.2019.01.004.
Polyak, S. L. 1941. "The Retina: The Anatomy and the Histology of the Retina in Man, Ape, and Monkey, Including the Consideration of Visual Functions, the History of Physiological Optics, and the Histological Laboratory Technique." *Chicago: University of Chicago Press*.
Polyak, Stephen. 1957. *The Vertebrate Visual System*. University of Chicago Press.
Silva, Susana da, and Constance L. Cepko. 2017. "Fgf8 Expression and Degradation of Retinoic Acid Are Required for Patterning a High-Acuity Area in the Retina." *Developmental Cell* 42 (1): 68-81.e6. https://doi.org/10.1016/j.devcel.2017.05.024.
Smallwood, Philip M., Yanshu Wang, and Jeremy Nathans. 2002. "Role of a Locus Control Region in the Mutually Exclusive Expression of Human Red and Green Cone Pigment Genes." *Proceedings of the National Academy of Sciences* 99 (2): 1008–11. https://doi.org/10.1073/pnas.022629799.
Sprecher, Simon G., and Claude Desplan. 2008. "Switch of Rhodopsin Expression in Terminally Differentiated Drosophila Sensory Neurons." *Nature* 454 (7203): 533–37. https://doi.org/10.1038/nature07062.
Szél, Ágoston, Theo van Veen, and Pál Röhlich. 1994. "Retinal Cone Differentiation." *Nature* 370 (6488): 336–336. https://doi.org/10.1038/370336a0.
Vollrath, Douglas, Jeremy Nathans, and Ronald W. Davis. 1988. "Tandem Array of Human Visual Pigment Genes at Xq28." *Science* 240 (4859): 1669–72. https://doi.org/10.1126/science.2837827.
Wahlin, Karl J., Julien A. Maruotti, Srinivasa R. Sripathi, John Ball, Juan M. Angueyra, Catherine Kim, Rhonda Grebe, Wei Li, Bryan W. Jones, and Donald J. Zack. 2017. "Photoreceptor Outer Segment-like Structures in Long-Term 3D Retinas from Human Pluripotent Stem Cells." *Scientific Reports* 7 (1): 766. https://doi.org/10.1038/s41598-017-00774-9.
Wald, George. 1967. "Blue-Blindness in the Normal Fovea*." *Journal of the Optical Society of America* 57 (11): 1289. https://doi.org/10.1364/JOSA.57.001289.
Wang, Yanshu, Jennifer P. Macke, Shannath L. Merbs, Donald J. Zack, Brenda Klaunberg, Jean Bennett, John Gearhart, and Jeremy Nathans. 1992. "A Locus Control Region Adjacent to the Human Red and Green Visual Pigment Genes." *Neuron* 9 (3): 429–40. https://doi.org/10.1016/0896-6273(92)90181-C.

Wang, Yanshu, Philip M. Smallwood, Mitra Cowan, Diane Blesh, Ann Lawler, and Jeremy Nathans. 1999. “Mutually Exclusive Expression of Human Red and Green Visual Pigment-Reporter Transgenes Occurs at High Frequency in Murine Cone Photoreceptors.” *Proceedings of the National Academy of Sciences* 96 (9): 5251–56. https://doi.org/10.1073/pnas.96.9.5251.

Wecker, Thomas, Bastian Grundel, Sabine Reichl, Milena Stech, Clemens Lange, Hansjürgen Agostini, Daniel Böhringer, and Andreas Stahl. 2019. “Anti-VEGF Injection Frequency Correlates with Visual Acuity Outcomes in pro Re Nata Neovascular AMD Treatment.” *Scientific Reports* 9 (1): 3301. https://doi.org/10.1038/s41598-019-38934-8.

Williams, David R., Donald I.A. MacLeod, and Mary M. Hayhoe. 1981. “Foveal Tritanopia.” *Vision Research* 21 (9): 1341–56. https://doi.org/10.1016/0042-6989(81)90241-8.

Willmer, E. N. 1944. “Colour of Small Objects.” *Nature* 153 (3895): 774–75. https://doi.org/10.1038/153774b0.

Willmer, E. N., and W. D. Wright. 1945. “Colour Sensitivity of the Fovea Centralis.” *Nature* 156 (3952): 119–21. https://doi.org/10.1038/156119a0.

Xiao, Ming, and Anita Hendrickson. 2000. “Spatial and Temporal Expression of Short, Long/Medium, or Both Opsins in Human Fetal Cones.” *J. Comp. Neurol*. Vol. 425.

Yi, Wenyang, Yufeng Lu, Suijuan Zhong, Mei Zhang, Le Sun, Hao Dong, Mengdi Wang, et al. 2020. “A Single-Cell Transcriptome Atlas of the Aging Human and Macaque Retina.” *National Science Review*, August. https://doi.org/10.1093/nsr/nwaa179.

Figure Legends

Fig 1. Human retina cone subtype specification across development
(A-C) Adult human retina photoreceptor pattern
(A) Human retina with boxed region representing macula. Red lines represent major arteries, pale lines represent major veins, white circle represents optic disc.
(B) Human macula with emphasis on macular subsections of the fovea and foveola.
(C) Photoreceptor composition of retinal regions with rods shown in grey, S cones shown in blue, and M/L cones shown in red. Highlighted regions from top to bottom include the periphery, the macula, the fovea, and the foveola.
(D) Representative images of S cones, M/L cones, and S+M/L cones from a retina at 14 weeks of gestation. Scale bar = 5 µm.
(E, I, M, P) Representation of cone patterning. Blue = regions of only S-only cones; purple = regions containing M/L-only and S+M/L co-expressing cones, and red = regions containing M/L-only cones. Solid lines indicate end of imaged region. Dotted lines indicate cuts in the tissue. Scale bar = 1.5 mm. (E) 10 weeks of gestation, (I) 12 weeks of gestation, (M) 14 weeks of gestation, (P) 16 weeks of gestation.
(F), (J), (N), (Q) Cone subtype composition by percent with S-only cones in blue, M/L-only and S+M/L co-expressing cones in purple, and M/L-only cones in red. “Low” indicates the region with the lowest S cone density. “High” indicates the region with the S cone density.
(G), (K), (O), (R) Cone subtype composition by density with S-only cones in blue, M/L-only and S+M/L co-expressing cones in purple, and M/L-only cones in red. “Low” indicates the region with the lowest S cone density. “High” indicates the region with the S cone density. “Average” indicates the average S cone density across all region.
(H, L) Heatmaps overlayed with the locations of each S cone observed at (E) 10 weeks of gestation and (I) 12 weeks of gestation.
(S) Summary of observations of S cone development in the presumptive foveola and periphery.

Fig 2. CYP26A1 and low RA limit S and promote M/L cone fate.
(**A-B**) Immunohistochemistry of day 204 organoids stained for S-opsin in blue and M/L-opsin in red. Scale bar = 25 µm.
(A) Control retinal organoid.
(B) *CYP26A1* mutant retinal organoid.
(C) % cone subtype per genotype (WT, N=3; *CYP26A1* mutant, N=3) with S-opsin in blue and M/L-opsin in red. Unpaired t test where P=0.0094.
(D) Cone subtype density per genotype (WT, N=3; *CYP26A1* mutant, N=3). Unpaired t test where P=0.0327.
(E) Model of the mechanism through which CYP26A1 promotes M/L cone fate.
(**F-H**) Immunohistochemistry of day 213 organoids stained for S-opsin in blue and M/L-opsin in red. Scale bar = 25 µm.
(F) 0 µM exogenous RA treated retinal organoid.
(G) 1 µM exogenous RA treated retinal organoid.
(H) 10 µM exogenous RA treated retinal organoid .
(I) % cone subtype per genotype. S cones in blue and M/L cones in red. One-way

ANOVA test with Dunnett correction. N = 5 organoids per condition.

Fig 3. Prolonged thyroid hormone (T3) converts S cones to M/L cones.
(**A-D**) Immunohistochemistry of day 204 organoids stained for S-opsin in blue (dashed line) and M/L-opsin (dotted line) in red. Cones co-expressing S- and M/L-opsin are outlined in a solid line. Scale bar = 25 μm.
(A) Control retinal organoid .
(B) 20 nM T3 from day 22-200.
(C) 20 nM T3 from day 22-152.
(D) 20 nM T3 from day 190-200.
(**E-F**) Cone subtype composition by density with S-opsin in blue and M/L-opsin in red and cones co-expressing S- and M/L-opsin in purple.
(E) Removal of 20 nM T3 at progressively later timepoints in retinal organoid differentiation. (N=3 for control and T3 day 22-200, N=4 for T3 day 152-200, T3 day 171-200, and T3 day 190-200).
(F) Addition of 20 nM T3 at progressively later timepoints in retinal organoid differentiation. (N=3 for control, T3 day 22-152, T3 day 22-190, and T3 day 22-200. N=4 for T3 day 22-172).

Fig 4. Model for foveolar cone patterning.
(A) Model: CYP26A1 represses RA to promotes M/L cone fate.
(B) Model: Prolonged DIO2 converts inactive T4 into active T3, converting S cones to M/L cone fate.
(C) Model of the temporal mechanism of foveolar cone subtype specification in humans.

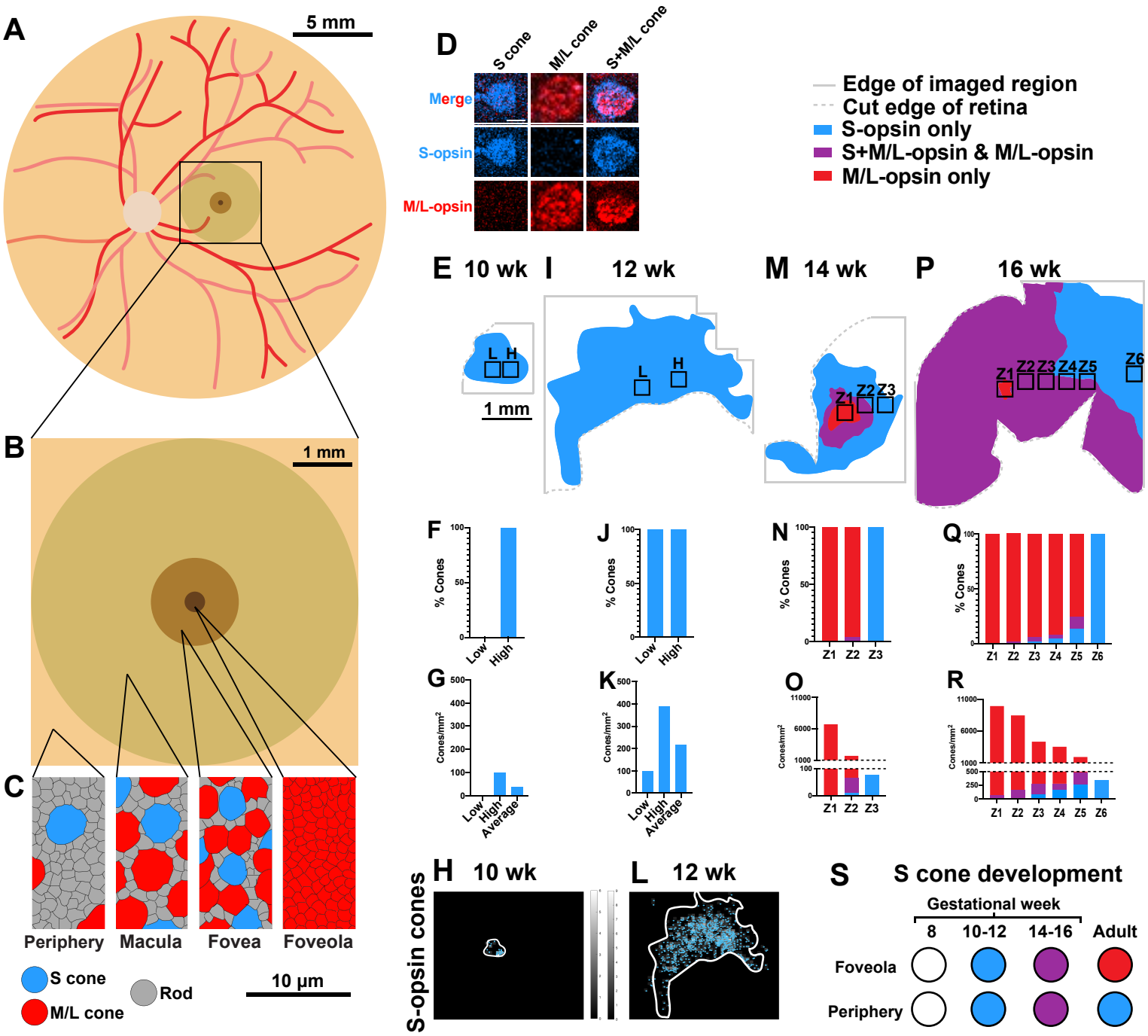
A
5 mm
B
1 mm
C
Periphery
Macula
Fovea
Foveola
S cone
M/L cone
Rod
10 µm
D
S cone
M/L cone
S+M/L cone
Merge
S-opsin
M/L-opsin
Edge of imaged region
Cut edge of retina
S-opsin only
S+M/L-opsin & M/L-opsin
M/L-opsin only
E 10 wk
I 12 wk
M 14 wk
P 16 wk
L H
1 mm
Z1 Z2 Z3
Z1 Z2 Z3 Z4 Z5 Z6
F
J
N
Q
% Cones
Low
High
Z1 Z2 Z3
Z1 Z2 Z3 Z4 Z5 Z6
G
K
O
R
Cones/mm²
Low
High
Average
H 10 wk
L 12 wk
S-opsin cones
S
S cone development
Gestational week
8
10-12
14-16
Adult
Foveola
Periphery

Figure 1

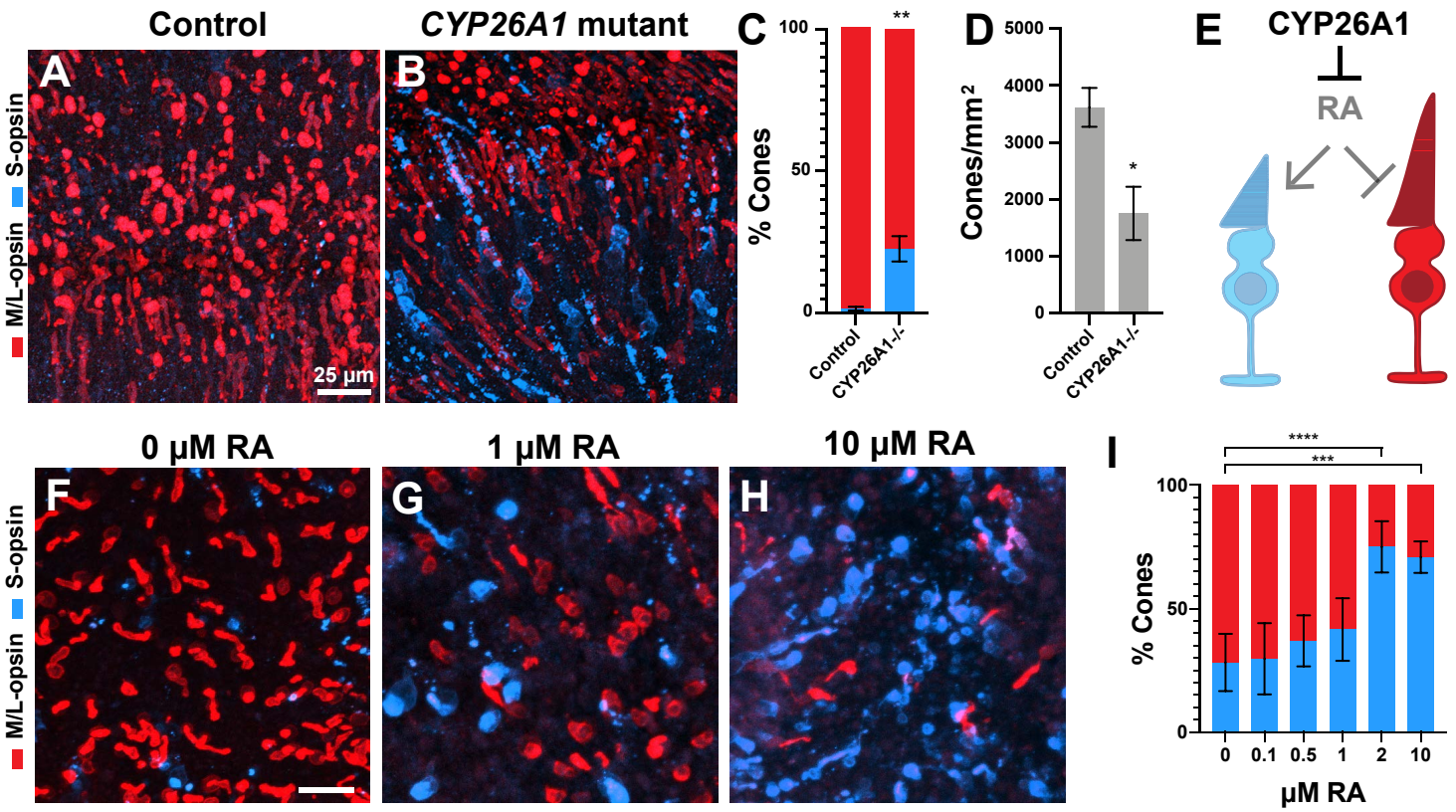
Control
CYP26A1 mutant
A
B
S-opsin
M/L-opsin
25 µm
C
% Cones
100
50
0
**
Control
CYP26A1-/-
D
Cones/mm²
5000
4000
3000
2000
1000
0
*
Control
CYP26A1-/-
E
CYP26A1
RA
0 µM RA
1 µM RA
10 µM RA
F
G
H
S-opsin
M/L-opsin
I
****
***
% Cones
100
50
0
0
0.1
0.5
1
2
10
µM RA

Figure 2

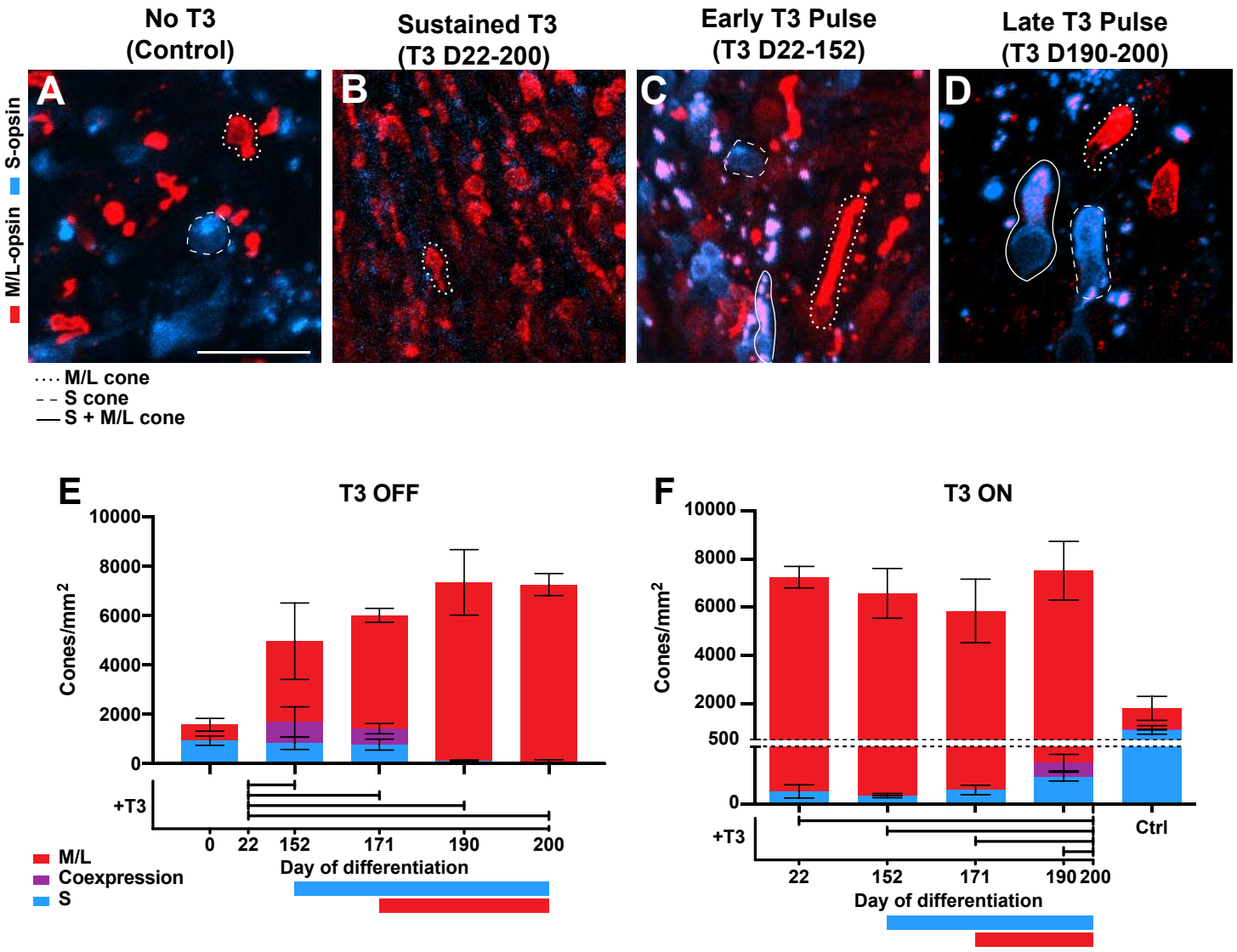
No T3
(Control)
Sustained T3
(T3 D22-200)
Early T3 Pulse
(T3 D22-152)
Late T3 Pulse
(T3 D190-200)
A
B
C
D
S-opsin
M/L-opsin
M/L cone
S cone
S + M/L cone
E
T3 OFF
Cones/mm2
10000
8000
6000
4000
2000
0
+T3
0
22
152
171
190
200
Day of differentiation
M/L
Coexpression
S
F
T3 ON
Cones/mm2
10000
8000
6000
4000
2000
500
0
+T3
22
152
171
190
200
Ctrl
Day of differentiation

Figure 3

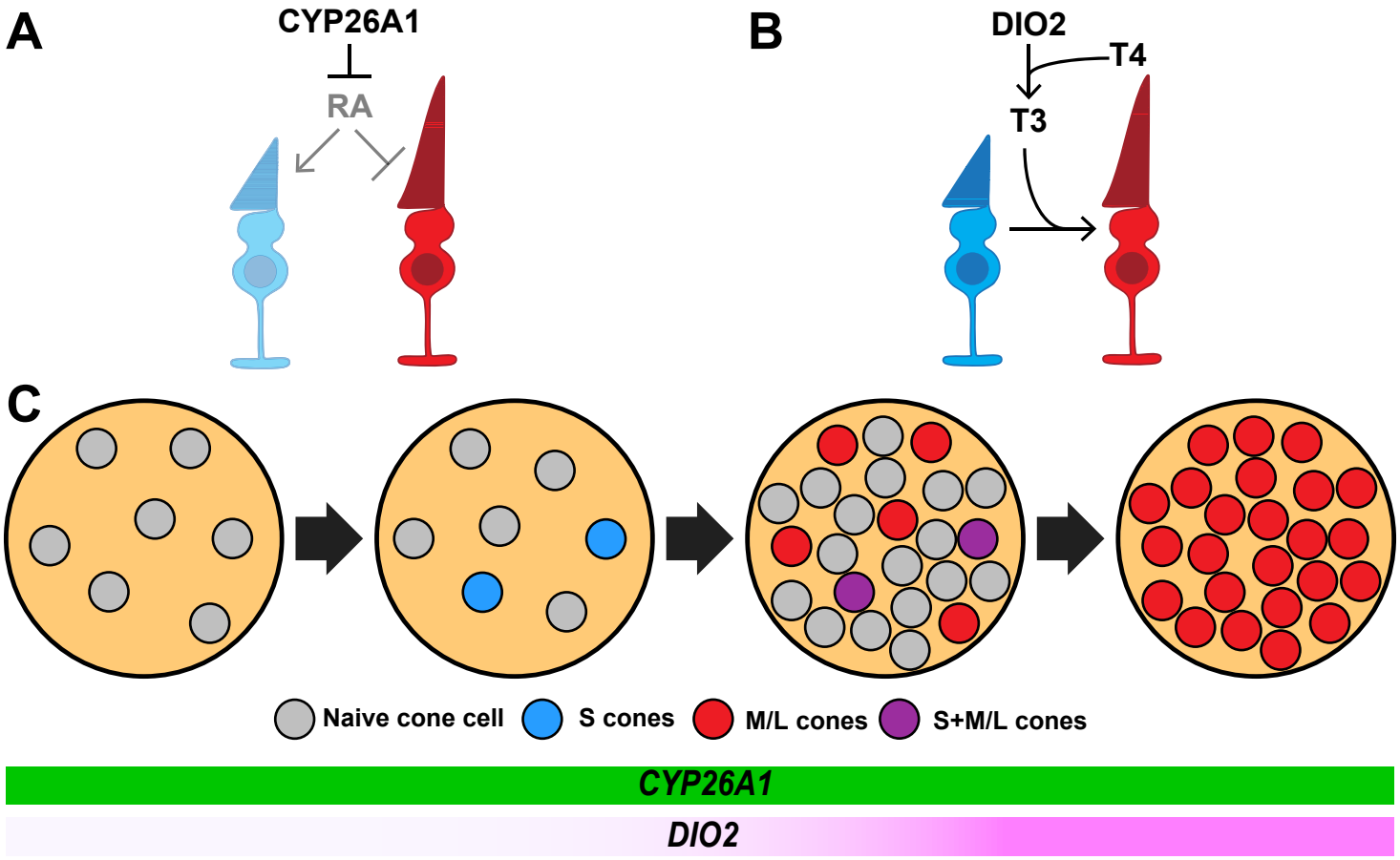
A
CYP26A1
RA
B
DIO2
T4
T3
C
Naive cone cell
S cones
M/L cones
S+M/L cones
CYP26A1
DIO2

Figure 4

Supplemental Fig 1. Distribution of S cones across development.
(**A-D**) Representation of cone patterning. Blue = regions of only S-only cones; purple = regions containing M/L-only and S+M/L co-expressing cones; and red = regions containing M/L-only cones. Solid lines indicate end of imaged region. Dotted lines indicate cuts in the tissue. Scale bar = 1.5 mm. Representative images of photoreceptors.
(E) Adult human retina from near foveola to far periphery. Scale bar = 800 µm. Boxes indicate representative zones quantified in I and J.
(F-H) Representative images of adult human retinal regions (F) near foveola, (G) in the mid-retina, (H) in the far periphery. Scale bar = 75 µm.
(I) Cone subtype composition of adult human retina by percent with S-only cones in blue, S+M/L co-expressing cones in purple, and M/L-only cones in red.
(J) Cone subtype composition of adult human retina by density with S-only cones in blue, S+M/L co-expressing cones in purple and M/L-only cones in red.

Supplemental Fig 2. Co-expression of S and M/L opsins during organoid development; CYP26A1 mutation; RA and cone densities.
(A-E) Time course of human retinal organoid cone subtype specification. S-opsin shown in blue, M/L-opsin shown in red, co-expression shown in purple. (N=3 for all timepoints). Scale bar = 25 µm.
(A) Retinal organoid at day 80.
(B) Retinal organoid at day 110.
(C) Retinal organoid at day 190.
(D) Cone subtype proportions during retinal organoid development.
(E) Cone subtype densities during retinal organoid development.
(F-G) Schematic of the CRISPR mutation generated in the CYP26A1 gene (E) Schematic depicting the entire gene where green squares are exons and green lines are introns. (F) Schematic depicting the nature of the mutation within exon 2 where green = unchanged, orange = deleted bases, yellow = a region of missense, and red = an early stop codon.
(**H**) Total cone density does not change significantly in different RA conditions. Related to Fig. 2I.

Supplemental Fig 3. Retinal organoid differentiation protocol.
Standard conditions for human retinal organoid differentiations as described in the materials and methods. Method adapted from (Wahlin et al. 2017; Eldred et al. 2018).

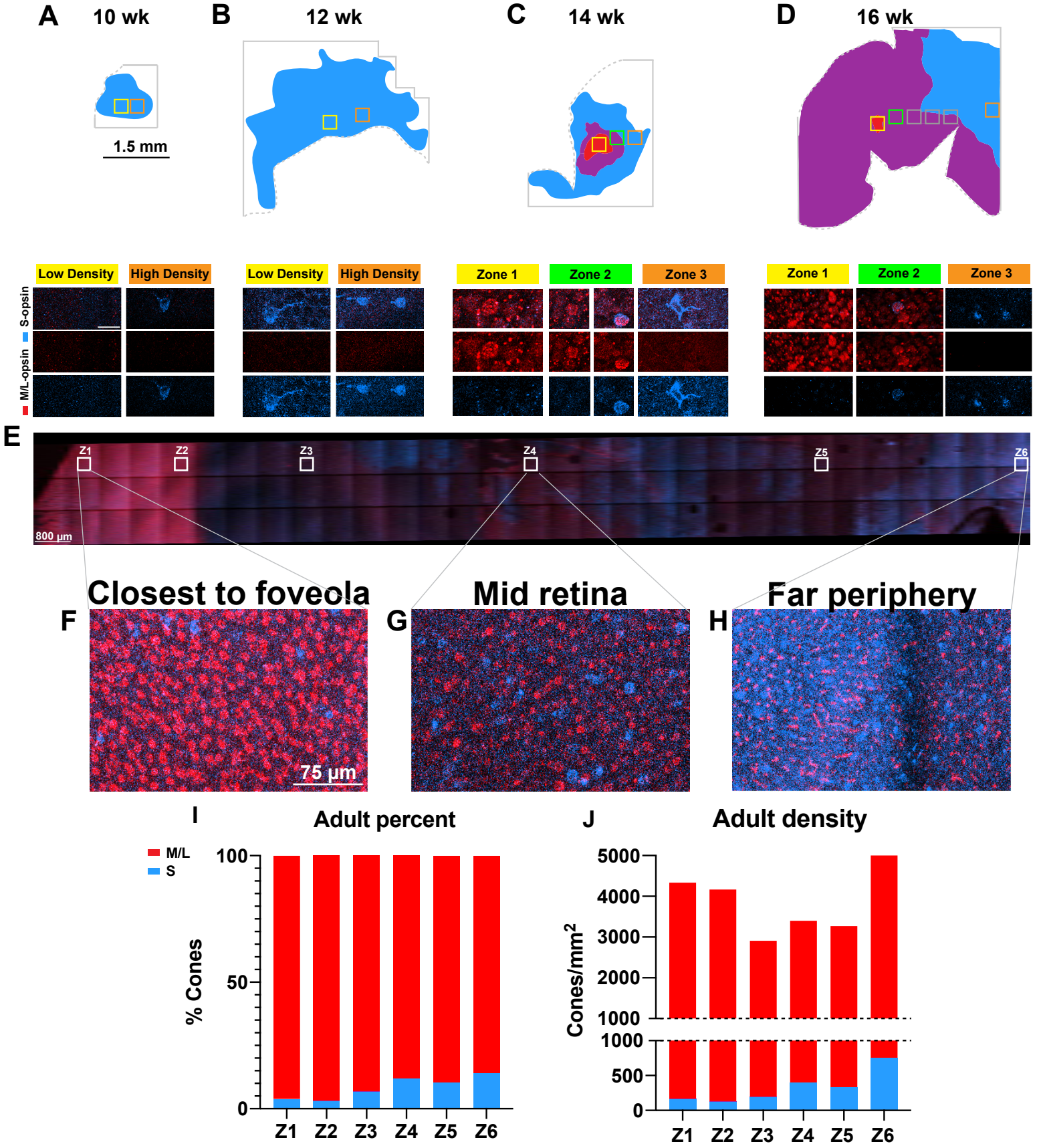

Supplemental Figure 1

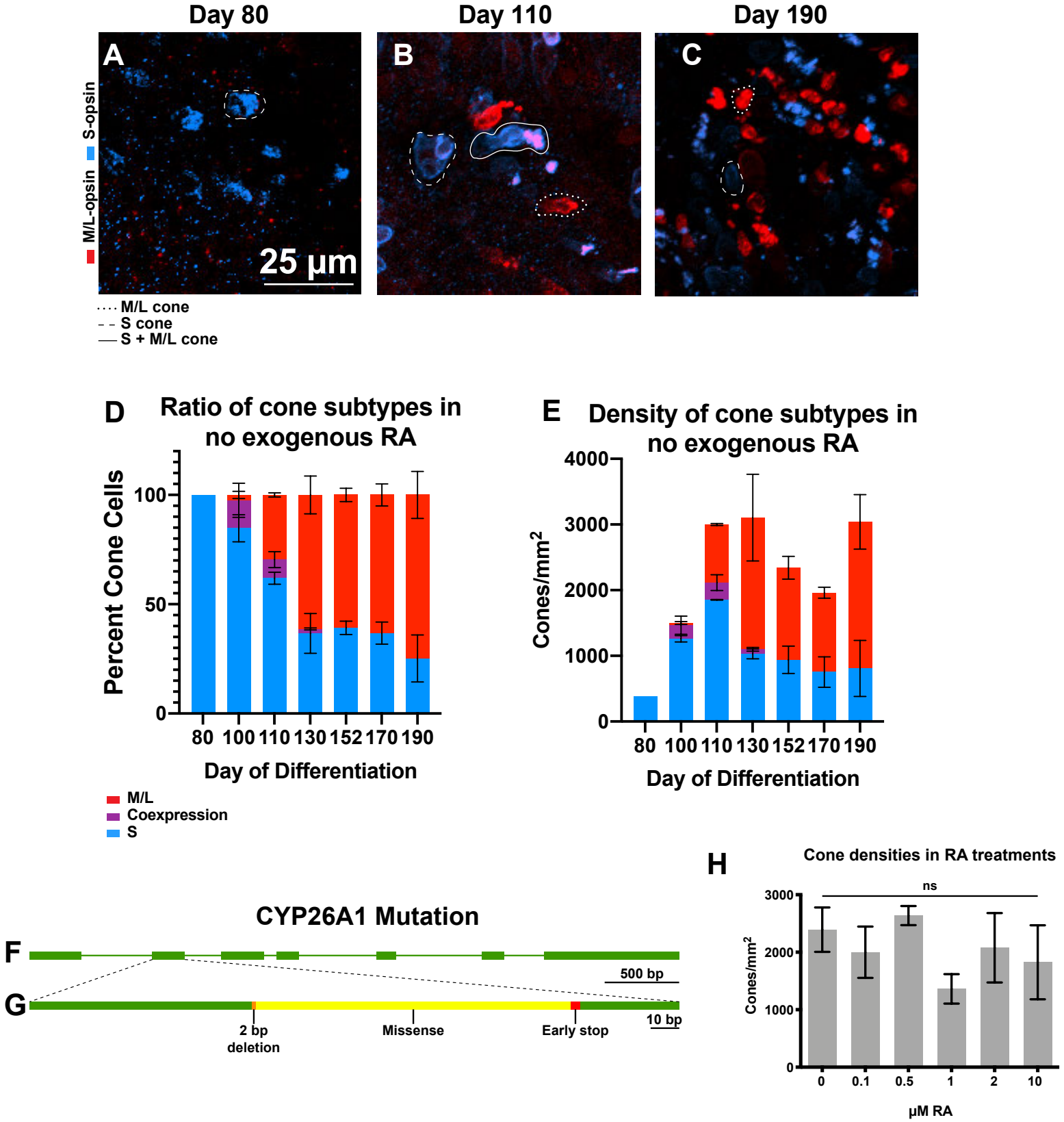

Supplemental Figure 2

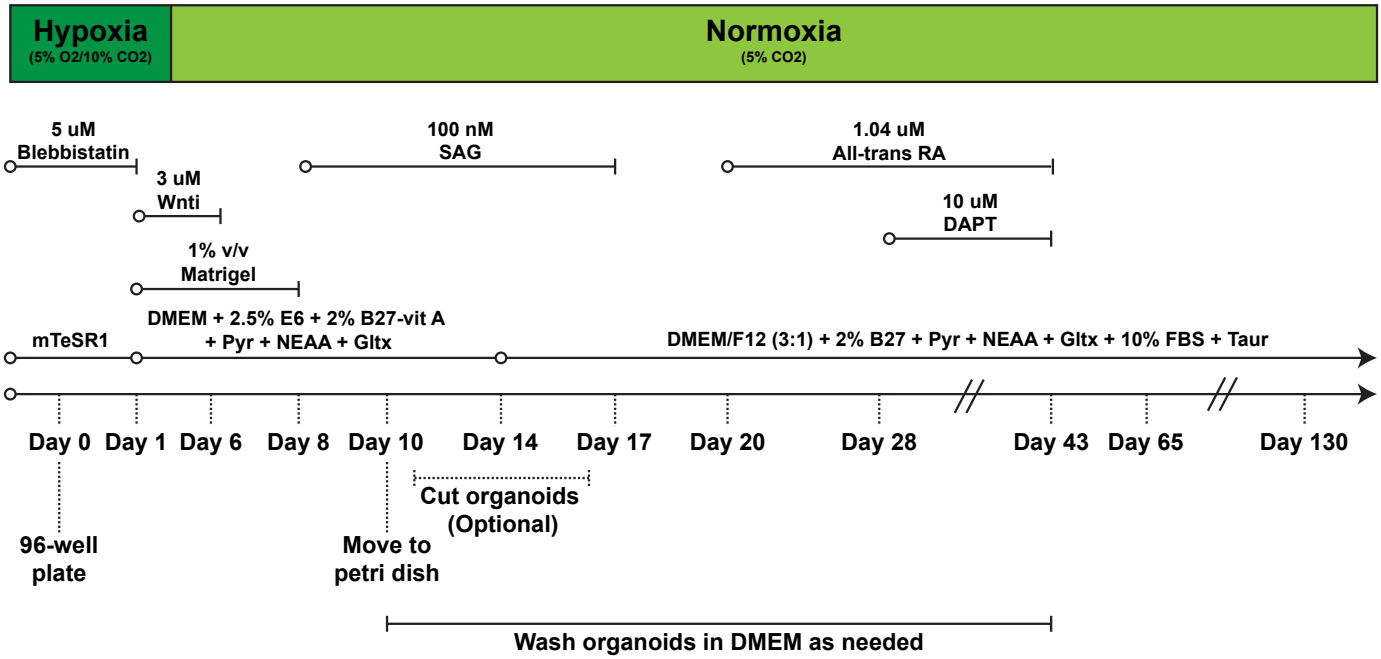

Supplemental Figure 3

Materials and Methods

Cell line maintenance

H7 ESC (WA07, WiCell) cells were used for differentiation. Stem cells were maintained in mTeSR™1 (85857, StemCell Technologies) on 1% (v/v) Matrigel-GFR™ (354230, BD Biosciences) coated dishes and grown at 37ºC in a HERAcell 150i or 160i 10% CO_2 and 5% O_2 incubator (Thermo Fisher Scientific). Cells were passaged every 4-5 days according to confluence as in (Wahlin et al. 2017). Cells were passaged with Accutase (SCR005, Sigma) for 7-12 minutes and dissociated to single cells. Cells in Accutase were added 1:2 to mTeSR™1 with 5 µM Blebbistatin (Bleb, B0560, Sigma), and pelleted at 150 g for 5 minutes. Cells were resuspended in mTeSR™1 with 5 µM Blebbistatin, density was quantified, and cells were plated at 5,000-15,000 cells per well in a prepared 6-well Matrigel coated plate. Cells were fed with mTeSR™1 48 hours after passaging and every subsequent 24 hours until passaged again. To minimize cell stress, no antibiotics were used. Cell lines were tested monthly for mycoplasma using MycoAlert (LT07, Lonza).

Cell culture media

Stem cell media: mTeSR™1 (85857, StemCell Technologies)

E6 supplement: 970 µg/mL Insulin (11376497001, Roche), 535 µg/mL holotransferrin (T0665, Sigma), 3.20 mg/mL L-ascorbic acid (A8960, Sigma), 0.7 µg/mL sodium selenite (S5261, Sigma).

BE6.2 media: 2.5% E6 supplement (above), 2% B27 supplement (50X) minus Vitamin A (12587010, Gibco), 1% Glutamax (35050061, Gibco), 1% NEAA (11140050, Gibco), 1 mM Sodium Pyruvate (11360070, Gibco), and 0.87 mg/mL NaCl in DMEM (11885084, Gibco).

LTR (Long-term retina) media: 25% F12 (11765062, Gibco), 2% B27 supplement (50X) (17504044, Gibco), 10% heat-inactivated FBS (16140071, Gibco), 1mM Sodium Pyruvate (11360070, Gibco), 1% NEAA (11140050, Gibco), 1% Glutamax (35050061, Gibco), and 1 mM taurine (T-8691, Sigma) in DMEM (11885084, Gibco).

Retinoic acid treatment: For organoids, stocks of 10.4 mM retinoic acid (ATRA; R2625, Sigma) were made in DMSO. Retinoic acid was then dissolved in LTR to reach desired working concentration.

Thyroid hormone treatment: For organoids, 20 nM T3 (T6397, Sigma) in LTR as used previously in mouse retinal explant culture (Roberts et al. 2006) and human retinal organoids (Eldred et al. 2018).

Organoid differentiation

Organoids were differentiated from H7 WA07 ESCs as described in (Wahlin et al. 2017; Eldred et al. 2018) (**Fig. S3**). Briefly, pluripotent stem cells were well-maintained, and only cultures with minimal to no spontaneous differentiation were used for aggregation. To aggregate, cells were passaged in Accutase at 37°C for 13 minutes to ensure complete single-cell dissociation. Cells were seeded in 50 uL of mTeSR™1 at 3,000 cells/well into 96-well ultra-low adhesion round-bottom Lipidure coated plates (51011610, NOF). Cells were placed in hypoxic conditions (10% CO2 and 5% O2) for 24 hours to enhance survival. Cells naturally aggregated by gravity over 24 hours.

On day 1, cells were moved to normoxic conditions (5% CO2). On days 1- 3, 50 uLs of BE6.2 media containing 3 μM Wnt inhibitor (IWR1e: 681669, EMD Millipore) and 1% (v/v) Matrigel were added to each well. On days 4-9, 100 uLs of media were removed from each well, and 100 uLs of media were replenished. On days 4-5, BE6.2 media containing 3 μM Wnt inhibitor and 1% Matrigel was added. On days 6-7, BE6.2 media containing 1% Matrigel was added. On days 8-9, BE6.2 media containing 1% Matrigel and 100 nM Smoothened agonist (SAG; 566660, EMD Millipore) was added.

On day 10, aggregates were transferred to 15 mL tubes, rinsed 2-3X in DMEM (11885084, Gibco), and resuspended in BE6.2 with 100 nM SAG in untreated 10 cm polystyrene petri dishes. From this point on, media was changed every other day. Aggregates were monitored daily and manually separated if stuck together or to the bottom of the plate.

On days 13-16, LTR media with 100 nM SAG was added.

Between days 11 and 16, retinal vesicles were optionally manually dissected if needed using sharpened tungsten needles. After dissection, cells were transferred into 15 mL tubes and washed 2X with 5 mLs of DMEM.

On days 16-20, cells were maintained in LTR and washed 2X with 5 mLs of DMEM, before being transferred to new plates to wash off dead cells. To increase survival and differentiation, 1 uM all-trans retinoic acid (ATRA; R2625; Sigma) was added to LTR medium from days 20-43 in all conditions. After day 43, retinoic acid was used at varying timings and concentrations depending on experimental conditions. 10 μM Gamma-secretase inhibitor (DAPT; 565770, EMD Millipore) was added to LTR from days 28-42. Organoids were grown at low density (10-20 per 10 cm dish, 2-3 per well in 6 well plate) to reduce aggregation. Organoids were regularly culled if failing to differentiate properly.

CRISPR mutations

Cloning gRNA plasmids: Plasmids for gRNA transfection were generated using pSpCas9(BB)-P2A-Puro plasmid modified from the pX459_V2.0 plasmid (62988, Addgene) by replacing T2A with a P2A sequence. gRNAs were cloned into the vector following the Zhang lab protocol:
https://pharm.ucsf.edu/sites/pharm.ucsf.edu/files/xinchen/media-browser/CRISPR%20cloning%20protocol%20Zhang%20Lab.pdf

gRNA Primer	Primer Sequence
CYP26A1 gRNA Forward	caccgTCCGCGCCCATCACCCGTA
CYP26A1 gRNA Reverse	aaacTACGGGTGATGGGCGCGGAc

Transfection and mutation identification: H7 stem cells were passaged in Accutase at 37°C for 13 minutes to ensure single-cell dissociation. Cells were seeded at 50,000 cells/well in a Matrigel-coated 24-well plate for 24 hours in mTeSR™1 with 5 μM Blebbistatin at hypoxic conditions. After 24 hours, media was removed and fresh mTeSR™1 was added. Cells were transfected with 2.5 uL Lipofectamine Stem Reagent (STEM00015, ThermoFisher Scientific), 200 ng gRNA plasmid PX459v2 containing the gRNA and Cas9-p2a-puromycin-resistance genes in 50 uL of Opti-MEM (31985062, Gibco). Cells were incubated for 24 hours, then media was removed and fresh mTeSR™1 was added. After 24 hours, media was removed and fresh mTeSR™1 along with 0.3-1

ug of puromycin (P8833, Sigma-Aldrich) was added to generate a kill curve. After 24 hours, media was removed and cells were washed 1X with mTeSR™1, then fresh mTeSR™1 was added to the wells. After several days, cells surviving at a puromycin concentration where all control cells had died were passaged at single cell density into a new, Matrigel-coated 6-well plate. Individual colonies were then isolated and mutations were confirmed by PCR sequencing. A gene diagram of the deletion is displayed in **Fig. S2F-G**.

Primer name	Primer sequence
CYP26A1 DL (PCR 1)	CATGCTATTGCGGCTAGGAG
CYP26A1 DR (PCR 1)	GGAATTCCGCTCATAAATGG
CYP26A1 L3 (PCR 2)	GATGAAGCGCAGGAAATACG
CYP26A1 R3 (PCR 2)	GCTTGTGCGAGGAGTCGT

Immunohistochemistry

Retinal organoids: Retinal organoids were fixed in fresh 4% formaldehyde and 5% sucrose in PBS for 50 minutes. Tissue was rinsed 3X in 5% sucrose in PBS, then incubated at 4°C in 6.75% sucrose in PBS for 30 min, 12.5% sucrose in PBS for 30 min, and 25% sucrose for 2 hours-overnight. Organoids were incubated for 2 hours-overnight at 4°C in blocking solution (0.2-0.3% Triton X100, 2-4% donkey serum in PBS). Organoids were incubated with primary antibodies in blocking solution for 16-36 hours at 4°C. Organoids were washed 3X for 15 minutes in PBS, and then incubated with secondary antibodies in blocking solution overnight at 4°C. Organoids were washed 3X for 10 minutes in PBS. Organoids were optionally incubated in 300 nM DAPI in blocking solution for 10 min and washed 3X for 15 min in PBS. At the end of staining, organoids were mounted for imaging in slow fade (S36940, Thermo Fisher Scientific).

Retinas: Human retinas were obtained from the National Disease Research Interchange (NDRI), the University of Maryland Brain and Tissue Bank, and the laboratory of Tom Reh. Human retinal tissue was in 10% formalin within 12 hours post-mortem and stored at 4°C until dissection. Retinas were dissected and whole-mounted, then rinsed 3X in PBS for 20 min, and blocked for 48 hours at 4°C in 0.3% Triton X-100 and 4% donkey serum. Retinas were stained with the same protocol as detailed above for organoids.

Antibodies

Primary antibodies were used at the following dilutions: goat anti-SWopsin (1:200 for organoids, 1:500 for human retinas) (sc-14363 Santa Cruz Biotechnology), chick anti-SWopsin (1:200 for organoids, 1:500 for human retinas) (gift from the laboratory of Jeremy Nathans) rabbit anti-LW/MW-opsins (1:200 for organoids, 1:500 for human retinas) (AB5405 Millipore), and mouse anti-Rhodopsin (1:500) (GTX23267 GeneTex). All secondary antibodies were Alexa Fluor-conjugated (1:400) and made in donkey (Molecular Probes).

Microscopy and image processing

Fluorescent images were acquired with a Zeiss LSM800 or LSM980 laser scanning confocal microscope. Confocal microscopy was performed with similar settings for laser

power, photomultiplier gain and offset, and pinhole diameter. Maximum intensity projections of z-stacks (5–150 optical sections, 1.00 μm step size) were rendered to display all cones captured in a single organoid.

Measurements and Quantification

Measurements of cone density were done using imageJ software. Quantifications and statistics (except for RNA-seq data) were done in GraphPad Prism, with a significance cutoff of 0.01. Statistical tests are listed in figure legends. All error bars represent the SEM. Organoids with < 150 total cones were deemed unhealthy and removed from our analysis.

References

Eldred, Kiara C., Sarah E. Hadyniak, Katarzyna A. Hussey, Boris Brenerman, Ping-Wu Zhang, Xitiz Chamling, Valentin M. Sluch, et al. 2018. “Thyroid Hormone Signaling Specifies Cone Subtypes in Human Retinal Organoids.” *Science* 362 (6411). https://doi.org/10.1126/science.aau6348.

Roberts, Melanie R., Maya Srinivas, Douglas Forrest, Gabriella Morreale de Escobar, and Thomas A. Reh. 2006. “Making the Gradient: Thyroid Hormone Regulates Cone Opsin Expression in the Developing Mouse Retina.” *Proceedings of the National Academy of Sciences* 103 (16): 6218–23. https://doi.org/10.1073/pnas.0509981103.

Wahlin, Karl J., Julien A. Maruotti, Srinivasa R. Sripathi, John Ball, Juan M. Angueyra, Catherine Kim, Rhonda Grebe, Wei Li, Bryan W. Jones, and Donald J. Zack. 2017. “Photoreceptor Outer Segment-like Structures in Long-Term 3D Retinas from Human Pluripotent Stem Cells.” *Scientific Reports* 7 (1): 766. https://doi.org/10.1038/s41598-017-00774-9.